THE JOURNAL OF BIOLOGICAL CHEMISTRY VOL. 286, NO. 52, pp. 45156–45164, December 30, 2011
© 2011 by The American Society for Biochemistry and Molecular Biology, Inc. Printed in the U.S.A.

Evidence against Cellular Internalization *in Vivo* of NMO-IgG, Aquaporin-4, and Excitatory Amino Acid Transporter 2 in Neuromyelitis Optica*

Received for publication, August 25, 2011, and in revised form, November 5, 2011 Published, JBC Papers in Press, November 8, 2011, DOI 10.1074/jbc.M111.297275

Julien Ratelade[‡], **Jeffrey L. Bennett**[§], **and A. S. Verkman**[‡1]

From the [‡]*Departments of Medicine and Physiology, University of California, San Francisco, California 94143 and the* [§]*Departments of Neurology and Ophthalmology, University of Colorado Denver, Aurora, Colorado 80045*

Background: Binding of the neuromyelitis optica (NMO) autoantibody (NMO-IgG) to aquaporin-4 (AQP4) is pathogenic in NMO.
Results: NMO-IgG binding does not cause endocytosis of itself, AQP4, or glutamate transporter EAAT2 in astrocyte cultures or *in vivo*.
Conclusion: Internalization of NMO-IgG, AQP4, and EAAT2 is not a significant feature of NMO.
Significance: Our results challenge a generally accepted paradigm on NMO pathogenesis.

Autoantibodies against astrocyte water channel aquaporin-4 (AQP4) are thought to be pathogenic in neuromyelitis optica (NMO). Prior work has suggested that a key component of NMO autoantibody (NMO-IgG) pathogenesis is internalization of AQP4 and the associated glutamate transporter EAAT2, leading to glutamate excitotoxicity. Here, we show selective endocytosis of NMO-IgG and AQP4 in transfected cell cultures, but little internalization in brain *in vivo*. AQP4-dependent endocytosis of NMO-IgG occurred rapidly in various AQP4-transfected cell lines, with efficient transport from early endosomes to lysosomes. Cell surface AQP4 was also reduced following NMO-IgG exposure. However, little or no internalization of NMO-IgG, AQP4, or EAAT2 was found in primary astrocyte cultures, nor was glutamate uptake affected by NMO-IgG exposure. Following injection of NMO-IgG into mouse brain, NMO-IgG binding and AQP4 expression showed a perivascular astrocyte distribution, without detectable cellular internalization over 24 h. We conclude that astrocyte endocytosis of NMO-IgG, AQP4, and EAAT2 is not a significant consequence of AQP4 autoantibody *in vivo*, challenging generally accepted views about NMO pathogenesis.

Neuromyelitis optica (NMO)[2] is an inflammatory disease of the central nervous system causing demyelinating lesions in spinal cord and optic nerve and to a lesser extent in brain (1, 2). A defining feature of NMO is the presence of autoantibodies in serum against astrocyte water channel aquaporin-4 (AQP4) (3, 4). NMO autoantibodies (NMO-IgG) are believed to be pathogenic by a mechanism involving complement- and cell-mediated cytotoxicity, elaboration of inflammatory mediators, and leukocyte accumulation (1, 5, 6). NMO lesions are characterized by loss of AQP4 and the astrocytic marker glial fibrillary acidic protein (GFAP), complement deposition, inflammation, and demyelination (1). NMO lesions are produced in mice administered NMO-IgG and complement by intracerebral injection (7), in rats with preexisting neuroinflammation administered NMO-IgG (8–10), and in spinal cord slice cultures exposed to NMO-IgG and complement (11). It is not known how NMO-IgG enters the central nervous system through an initially intact blood-brain barrier or why NMO-IgG does not cause pathology in peripheral tissues where AQP4 is expressed. Another unresolved aspect of NMO pathology is how NMO-IgG-induced primary astrocyte injury leads to demyelination and neuronal impairment.

NMO-IgG-dependent astrocyte pathology requires AQP4 exposure on the cell surface to bind and activate complement and cytotoxic leukocytes. Paradoxically, prior studies showed rapid internalization *in vitro* of AQP4 in response to NMO serum (12–14), which, rather than promoting NMO pathogenesis, would protect astrocytes from cytotoxicity. One study also reported internalization of glutamate transporter EAAT2 together with AQP4 (13) and concluded that NMO pathogenesis involves glutamate excitotoxicity by a mechanism involving NMO-IgG-induced internalization of EAAT2 and consequent impairment in glutamate uptake from the extracellular space following neuroexcitation. Marignier *et al.* (15) showed that elevated extracellular glutamate could injure oligodendrocytes in an astrocyte/oligodendrocyte mixed primary cell culture. They suggested glutamate excitotoxicity as a possible cause of demyelination in NMO. Based on this mechanism, ceftriaxone, which up-regulates EAAT2 (16), has been proposed as a therapy for NMO.

Cellular internalization of AQP4, EAAT2, and NMO-IgG, if it occurs in the CNS *in vivo*, would have important implications

* This work was supported, in whole or in part, by National Institutes of Health Grants EY13574, EB00415, DK35124, HL73856, DK86125 and DK72517 (to A. S. V.). This work was also supported by grants from the Guthy-Jackson Charitable Foundation (to A. S. V. and J. L. B.) and Grant RG4320 from the National Multiple Sclerosis Society (to J. L. B.).

[1] To whom correspondence should be addressed: 1246 Health Sciences East Tower, University of California, San Francisco, CA 94143-0521. Tel.: 415-476-8530; Fax: 415-665-3847; E-mail: alan.verkman@ucsf.edu.

[2] The abbreviations used are: NMO, neuromyelitis optica; AQP4, aquaporin-4; EAAT2, excitatory amino acid transporter 2; GFAP, glial fibrillary acidic protein; NMO-IgG, NMO autoantibody; FRT cell, Fischer rat thyroid epithelial cell; PFA, paraformaldehyde; rAb, recombinant antibody; WGA, wheat germ agglutinin.

for NMO pathogenesis and therapy (see "Discussion"). Here, quantitative biophysical and biochemical assays of internalization were done in cell cultures and in live mice, utilizing for some studies a fluorescently labeled monoclonal recombinant NMO-IgG for real time antibody tracking in live cells. We found rapid and selective internalization of NMO-IgG and AQP4 in transfected cell cultures, but little or no internalization of NMO-IgG, AQP4, or EAAT2 in primary astrocytes, or of NMO-IgG and AQP4 in brain. Our results thus challenge a widely cited view of NMO disease pathogenesis.

EXPERIMENTAL PROCEDURES

Mice—AQP4-null mice were generated previously by targeted gene disruption (17). Experiments were done on weight-matched wild-type and null mice on a CD1 genetic background (age 16–18 weeks). Mice were maintained in air-filtered cages and fed normal mouse chow in the University of California San Francisco (U.C.S.F.) Animal Care Facility. All procedures were approved by the U.C.S.F. Committee on Animal Research.

NMO Antibody and DNA Constructs—Purified human monoclonal NMO-IgG rAb-53 was generated as described (8), with a measles virus-specific rAb (2B4) used as an isotype-matched control. Fluorescent labeling of rAb-53 with Cy3 (rAb-53-Cy3) and of a Myc antibody (Santa Cruz Biotechnology, Santa Cruz, CA) was done using the Amersham Biosciences Cy3 Ab Labeling Kit (GE Healthcare). DNA constructs encoding full-length human AQP4 (M1 and M23 isoforms) were generated by PCR amplification using whole brain cDNA as template. For some studies a Myc epitope (NH_2-EQKLISEEDL-COOH) was inserted in the second extracellular loop by PCR amplification using the nontagged constructs as template, as described (18). PCR fragments were ligated into mammalian expression vector pcDNA3.1 and sequenced. IgGs from NMO patient serum and from normal human serum were purified using the Melon™ Gel IgG purification kit (Thermo Scientific).

Cell Culture and Transfections—Chinese hamster ovary cells (CHO-K1; ATCC CCL-61), Fischer rat thyroid epithelial cells (FRT; ATCC CRL-1468), and human glioblastoma cells (U87-MG; ATCC HTB-14) were cultured at 37 °C in 5% CO_2/95% air in F12 Ham's medium, F12 Coon's modified medium, and DMEM H21 (Sigma-Aldrich), respectively, containing 10% FBS, 100 units/ml penicillin, and 0.1 mg/ml streptomycin. Cells were grown on glass coverslips and transfected with DNAs in antibiotic-free medium using Lipofectamine 2000 (Invitrogen) according to the manufacturer's protocol. Stable AQP4-expressing clones were selected following enrichment in Geneticin (Invitrogen) and plating in 96-well plates at low density. Primary astrocyte cultures were generated from cortex of wild-type and AQP4-null neonatal mice, as described (19). After 8–10 days in culture, cells were treated for 2 weeks with 0.25 mM dibutyryl cAMP (Sigma-Aldrich) to induce differentiation. Immunocytochemistry showed that >95% of cells were positive for the astrocyte marker GFAP.

NMO-IgG Internalization Assay—Cells were grown on coverglasses until confluent. Cells were washed twice with PBS supplemented with 6 mM glucose and 1.1 mg/ml sodium pyruvate (PBS^+) and incubated for 20 min in PBS^+ containing 1% BSA at room temperature. Cells were subsequently labeled with rAb-53-Cy3 (10 μg/ml) at 4 °C for 1 h. Following extensive washing with cold PBS^+, cells were chased at 37 °C for specified times. Coverglasses were mounted in an open chamber, and fluorescence was measured using an inverted epifluorescence microscope (Eclipse TE2000-E, Nikon) with a Nikon oil immersion 100×, NA 1.49 Apo TIRF objective lens. Fluorescence images were obtained before and after addition of the dark quencher bromocresol green (final concentration 4 mM) in the cell-bathing solution (29). In some experiments, AQP4-expressing cells were chased for 3 h at 37 °C and labeled with the lysosomal marker lysosensor green (1:4,000; Invitrogen) for 5 min. In another set of experiments, cells were fixed, permeabilized, and stained with a rabbit antibody against the early endosome antigen 1 (EEA1) (1:100; Abcam, Cambridge, MA). As a positive control of internalization, astrocytes were incubated for 1 h at 37 °C with 6 μM Texas Red hydrazide (Invitrogen), a dye preferentially internalized by astrocytes (21), or with 0.1 mg/ml fluorescein-transferrin (Invitrogen).

Quantification of Cell Surface AQP4—AQP4-transfected cells and mouse primary astrocytes were grown on coverglasses until confluent and incubated for specified times with 50 μg/ml rAb-53 at 37 °C. Cells were then washed extensively in cold PBS^+ and blocked for 20 min in 1% BSA at 4 °C. Remaining AQP4 at the cell surface was labeled with 50 μg/ml rAb-53 at 4 °C for 1 h. Subsequently, rAb-53 was labeled by incubation for 1 h at 4 °C with goat anti-human IgG-conjugated Alexa Fluor 555 (1:200, Invitrogen), and the plasma membrane was stained using a fluorescent lectin, wheat germ agglutinin (WGA)-conjugated Alexa Fluor 488 (1:400; Invitrogen). Cells were then washed in cold PBS^+ and fixed for 15 min in 4% paraformaldehyde (PFA). Surface AQP4 was quantified as the (background-subtracted) ratio of red (surface AQP4) to green (plasma membrane) fluorescence using ImageJ. In some experiments, surface AQP4 in astrocytes was measured using the same assay following exposure for 24 h to 5 mg/ml IgG purified from NMO or control sera. Before labeling of surface AQP4 with rAb-53, bound IgG at the cell surface were removed by acid wash in 0.2 M glycine, pH 2.5, for 15 s. In another set of experiments, astrocyte cultures were fixed and permeabilized following exposure to rAb-53 and stained with a rabbit anti-EAAT2 antibody directed against a C-terminal epitope (1:100; Cell Signaling Technology).

Glutamate Uptake Assay—EAAT2 expression in mouse primary astrocytes was verified by immunoblotting cell lysates using a rabbit anti-EAAT2 antibody (1:1,000; Cell Signaling Technology) and a HRP-conjugated anti-rabbit antibody (1:10,000; Santa Cruz Biotechnology). Mouse primary astrocyte cultures were grown in 24-well dishes and preincubated with 50 μg/ml rAb-53 or control IgG for 24 h at 37 °C. Cells were subsequently washed in PBS and incubated at 37 °C in 120 mM NaCl, 25 mM Tris, 5 mM KCl, 1 mM KH_2PO_4, 1 mM $MgSO_4$, 2 mM $CaCl_2$, 10 mM D-glucose, pH 7.4, containing 200 μM glutamate and the corresponding antibody. In some measurements 120 mM NaCl was replaced with 120 mM choline chloride to determine Na^+-dependent glutamate uptake. After 1 h at 37 °C, medium was removed, and glutamate concentration was quan-

tified using a Glutamate Assay Kit (BioVision, Mountain, View, CA) according to the manufacturer's protocol.

In Vivo Injection of NMO-IgG—For brain injection, mice were anesthetized using 2,2,2-tribromoethanol (250 mg/kg intraperitoneally; Sigma-Aldrich) and mounted onto a stereotaxic frame. A midline scalp incision was made, and a burr hole of diameter 1 mm was drilled in the skull 1 mm to the right and 1 mm posterior to bregma. A 30-g needle attached to a 50-μl gas-tight glass syringe (Hamilton, Reno, NV) was inserted 3 mm deep to infuse 5 μg of rAb-53-Cy3 or unlabeled rAb-53 in a volume of 5 μl (~1 μl/min). In some experiments, 5 μl of 12 μM Texas Red hydrazide or 5 μl of control antibody 2B4 (1 mg/ml) was injected into the brain by the same method. rAb-53 injections were also performed in AQP4-null mice. In some experiments, 150 μg of purified IgG from NMO or control sera was injected in the same volume. At specified times after injection, mice were anesthetized and perfused through the left cardiac ventricle with 10 ml of PBS and then 10 ml of PBS containing 4% PFA. Brains were postfixed for 2 h in 4% PFA and dehydrated overnight in 30% sucrose at 4 °C. Tissues were embedded and frozen in O.C.T. compound (Sakura Finetek, Torrance, CA) for sectioning and immunostaining. Brains injected with rAb-53-Cy3 were postfixed in 4% PFA for 2 h, dehydrated in 70% ethanol, and embedded in paraffin.

Tissue Immunofluorescence—Ten-μm-thick frozen sections or 5-μm-thick paraffin sections were blocked for 1 h in PBS containing 10% goat serum (blocking buffer) and incubated for 1 h at room temperature with the following primary antibodies diluted in blocking buffer: rabbit anti-AQP4 (1:50; Santa Cruz Biotechnology), mouse anti-GFAP (1:100; Millipore), or rat anti-CD31 (1:50; BD Biosciences). Sections were washed with PBS and incubated for 1 h with the corresponding goat IgG-conjugated Alexa Fluor secondary antibodies (1:200; Invitrogen). Unlabeled rAb-53 and purified serum IgGs were detected using goat anti-human IgG-conjugated Alexa Fluor 555 or 488 (1:200; Invitrogen). Sections were then washed with PBS and mounted in Vectashield medium (Vector Laboratories, Burlingame, CA). Sections were imaged using a laser scanning confocal microscope equipped with a Nikon 100×, NA 1.49 Apo TIRF objective lens.

RESULTS

rAb-53 Is Internalized in AQP4-transfected cells and Targeted to Lysosomes—NMO-IgG cellular processing was studied using a purified, recombinant monoclonal human antibody (rAb-53) generated from paired heavy and light chain sequences cloned from cerebrospinal fluid plasma blasts of a NMO patient (8). This antibody binds strongly to human and mouse AQP4 and causes antibody-dependent complement-mediated lysis and cellular cytotoxicity (8, 22). Antibody rAb-53 also binds the two major isoforms of AQP4, M1 and M23, which are expressed in astrocytes, with greater affinity for AQP4-M23 (22). The M23 isoform of AQP4 forms supramolecular assemblies in cell plasma membranes called orthogonal arrays of particles, whereas M1 does not (23). To image its internalization, rAb-53 was labeled with the red fluorophore Cy3 (rAb-53-Cy3) under conditions that do not affect its binding to AQP4. A dark quencher of Cy3 fluorescence (29), bromocresol green, was used to distinguish surface-bound from internalized rAb-53-Cy3 because it does not permeate into cells and reduces by >98% the fluorescence of Cy3.

CHO cells stably expressing human AQP4-M23 were labeled with rAb-53-Cy3 at 4 °C, washed, and chased at 37 °C (Fig. 1*A*). Fig. 1*B* shows localization of rAb-53-Cy3 exclusively at the cell surface at 0 time, just after 4 °C labeling, as seen by its membrane expression pattern and loss of fluorescence following quencher addition. Binding of rAb-53-Cy3 was AQP4-dependent, as no fluorescence was seen in nontransfected cells (data not shown). At 15-min and 1-h chase times there was progressive rAb-53-Cy3 internalization that was essentially complete by 1 h, as seen by the lack of effect of quencher. At 15-min chase time rAb-53-Cy3 (*red*) colocalized with the early endosomal marker EEA1 (*green*) (Fig. 1*C*, *left*) and at 3 h with a lysosomal marker (*green*) (Fig. 1*C*, *right*). Binding of rAb-53-Cy3 to AQP4-M23 in transfected cells thus results in its efficient endocytosis and targeting to lysosomes.

Surface AQP4 Is Decreased in AQP4-transfected Cells Exposed to NMO-IgG—The efficient cellular internalization of AQP4-bound NMO-IgG is predicted to reduce AQP4 surface expression in the steady state if NMO-IgG-induced AQP4 internalization exceeds AQP4 exocytosis. AQP4-M23-transfected cells were incubated with a high concentration of rAb-53 at 37 °C allowing binding and internalization of the antibody and AQP4. At specified times, cells were washed, cooled to 4 °C to block endocytosis, and the remaining AQP4 at the surface was labeled using rAb-53 and a red fluorescent secondary antibody (Fig. 2*A*). The cell surface was labeled green with a fluorescent conjugate of the lectin WGA. Fig. 2*B* shows rapid reduction in cell surface AQP4 (*red*) following 37 °C chase in the presence of rAb-53, with >50% reduction in surface AQP4 at 15 min as quantified by the red-to-green fluorescence ratio (Fig. 2*D*). Cell surface AQP4 was not reduced in studies done using a control (non-NMO) antibody (Fig. 2, *C* and *D*).

NMO-IgG Internalization in Transfected Cells Is Specific and Isoform- and Cell Type-independent—To determine whether NMO-IgG endocytosis is AQP4 isoform- and cell type-specific, measurements of rAb-53-Cy3 internalization were done, as in Fig. 1, but for CHO cells transfected with the M1 isoform of AQP4, and for U87 (of human astrocyte origin) and FRT (epithelial cell type) cells transfected with AQP4-M23. rAb-53-Cy3 was efficiently internalized in the AQP4-M1-expressing CHO cells (Fig. 3*A*) as well as in the AQP4-M23-expressing U87 (Fig. 3*B*) and FRT (Fig. 3*C*) cells. Thus, rAb-53 internalization in transfected cells is not specific to AQP4 isoform or cell type.

To investigate whether the rapid internalization of NMO-IgG is antibody-specific, we measured the internalization of a Cy3-labeled anti-Myc antibody in CHO cells expressing an epitope-tagged AQP4 in which a Myc sequence was inserted into the second extracellular loop of AQP4. We showed previously that the Myc insertion does not affect AQP4 cellular processing or water permeability (18). In contrast to the results for rAb-53-Cy3, no detectable internalization of the Myc antibody was found (Fig. 3*D*), indicating specificity for NMO-IgG internalization.

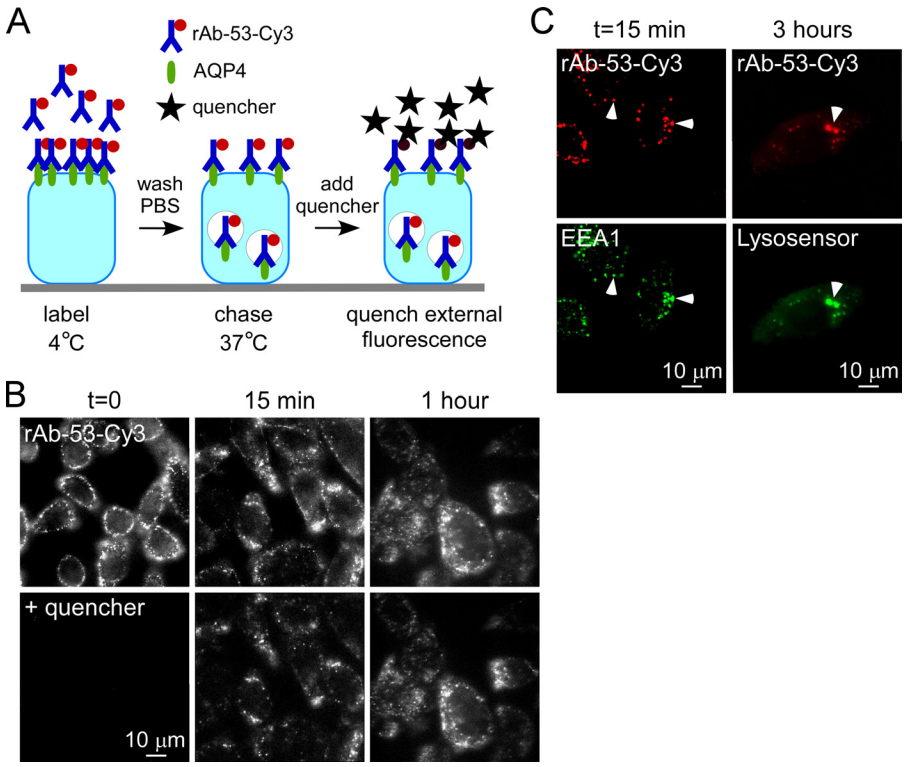

FIGURE 1. **Rapid endocytosis of rAb-53 in CHO cells stably transfected with AQP4.** *A*, schematic of internalization assay. CHO cells stably expressing AQP4 (M23 isoform) were labeled with rAb-53-Cy3 at 4 °C, washed, and chased at 37 °C for specified times. Fluorescence of rAb-53-Cy3 remaining at the cell surface was quenched with the dark quencher bromocresol green. *B*, rAb-53-Cy3 fluorescence before and after addition of quencher at the indicated chase times. Micrographs are representative of four separate sets of experiments. *C*, colocalization (*arrowheads*) of rAb-53-Cy3 (*red*) with the early endosome marker EEA1 (*green*) at 15-min chase and with a lysosomal marker (*green*) at 3-h chase.

NMO-IgG, AQP4, and EAAT2 Are Not Internalized in Primary Astrocyte Cultures—To determine whether NMO-IgG is internalized in a more relevant cell type to NMO pathology, we measured internalization in primary, well differentiated cultures of mouse astrocytes. Fig. 4*A* shows binding of rAb-53-Cy3 (*red*) to AQP4 (*green*) on astrocytes from wild type (+/+) mice. No binding was seen on astrocytes from AQP4 null (−/−) mice. Internalization of rAb-53-Cy3 was assayed as described above. Following labeling at 4 °C, rAb-53-Cy3 was localized at the cell surface, as fluorescence was absent after quencher addition (Fig. 4*B*, *left*). After a 1-h chase, little antibody was internalized as nearly all fluorescence was quenched (Fig. 4*B*, *middle*). We verified active endocytosis in the astrocytes studied here by incubation for 1 h at 37 °C with Texas Red hydrazide, a fluid phase marker of endocytosis, and fluorescein-transferrin, a marker of receptor-mediated endocytosis (Fig. 4*B*, *right*).

Cell surface AQP4 on astrocytes was also measured following rAb-53 exposure. Cell surface AQP4 was not reduced significantly as quantified by red-to-green fluorescence ratios (Fig. 4*C*).

We also studied the cellular localization of the Na^+-dependent glutamate transporter EAAT2, which is expressed endogenously in astrocytes (24). By confocal immunofluorescence of fixed, permeabilized cells using an EAAT2 antibody directed against an intracellular epitope, EAAT2 was seen mainly at the plasma membrane (Fig. 4*D*, *left*). Following incubation with rAb-53 for 3 h at 37 °C, the plasma membrane localization of EAAT2 was not changed (Fig. 4*D*, *right*). Immunoblotting confirmed EAAT2 antibody specificity (Fig. 4*D*, *bottom*). As a functional measure of EAAT2 plasma membrane expression, Na^+-dependent glutamate uptake was measured in astrocytes following incubation with rAb-53 or control IgG. Na^+-dependent glutamate uptake was not reduced significantly in the rAb-53-incubated astrocytes (Fig. 4*E*). Together, these results indicate that exposure of astrocytes to NMO-IgG does not cause internalization of itself, nor of AQP4 or EAAT2.

Little Internalization of NMO-IgG and AQP4 in Mouse Brain in Vivo—To study the cellular processing of NMO-IgG *in vivo*, confocal microscopy was used to determine the localization of rAb-53-Cy3 after direct injection into brain parenchyma. Fig. 5*A* shows the spatial distribution of rAb-53-Cy3 in brain at 3 h after injection, showing diffusion up to 2 mm from the injection site. Localization of the rAb-53-Cy3 was assessed in an area (*white square*) near the needle tract. Fig. 5*B* (*left*) shows perivascular colocalization of rAb-53-Cy3 and AQP4 in brain of wild-type mice at 3 h after injection. Selective antibody localization was not seen for control (non-NMO) IgG (*middle*) nor for rAb-53-Cy3 in brain of AQP4 knock-out mice (*right*). Fig. 5*C* shows similar perivascular localization of rAb-53-Cy3 and AQP4 at 20 min and 1, 3, and 24 h after injection, suggesting little cellular internalization in astrocytes in brain.

Colocalization studies support the conclusion that rAb-53-Cy3 and AQP4 are not internalized in astrocytes in brain *in vivo*. Fig. 6*A* shows costaining for the astrocytic cytoplasmic marker GFAP (*green*) and rAb-53-Cy3 (*red*) at different times after injection. At each time point rAb-53-Cy3 was localized to astrocyte foot processes surrounding blood vessels, whereas GFAP stained the whole astrocyte bodies, whose extensions

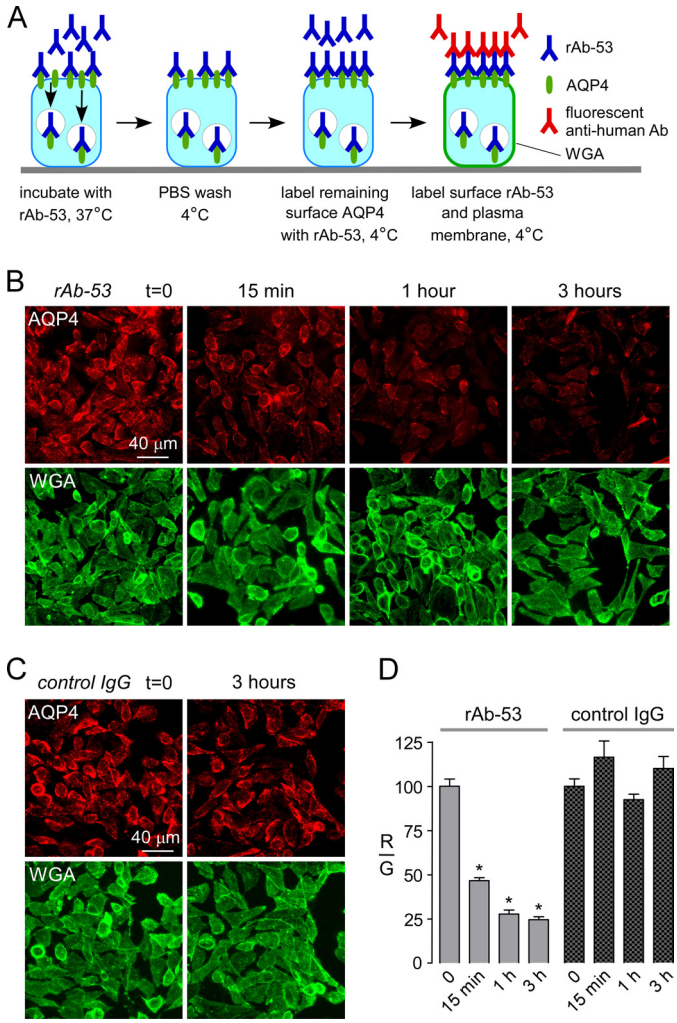

FIGURE 2. **Reduced cell surface AQP4 in AQP4-transfected CHO cells following rAb-53 exposure.** *A*, schematic of assay. CHO cells stably expressing AQP4 (M23 isoform) were incubated for specified times with rAb-53 at 37 °C, washed, cooled to 4 °C, and assayed for cell surface AQP4 by addition of rAb-53 and fluorescent secondary antibody. Plasma membrane was stained green with fluorescent WGA. *B*, cells stained for surface AQP4 (*red*) and plasma membrane (WGA, *green*) following incubation with rAb-53 for the indicated times. *C*, experiments as in *B* except that cells were incubated with a control (non-NMO) IgG. *D*, quantification of surface AQP4 from ratio of (background-subtracted) red-to-green fluorescence (*R*/*G*, mean ± S.E. (*error bars*), $n = 10$; *, $p < 0.01$). Results are representative of two sets of experiments.

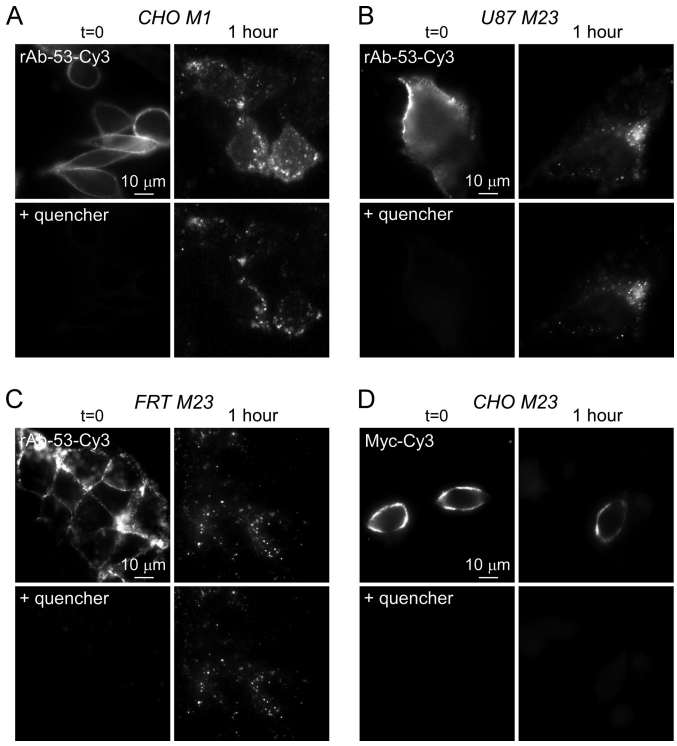

FIGURE 3. **Specificity of rAb-53 internalization in AQP4-transfected cell cultures.** *A–C*, Cy3 fluorescence before and after addition of quencher, showing internalization of rAb-53-Cy3 at 1-h chase in CHO cells expressing AQP4-M1 (*A*), U87 cells expressing AQP4-M23 (*B*), and FRT cells expressing AQP4-M23 (*C*). *D*, same internalization assay (1-h chase) in CHO cells expressing AQP4-M23 containing a Myc epitope inserted in its second extracellular loop and with a Cy3-labeled anti-Myc antibody. Results are representative of three sets of experiments.

project into the perivascular space. Staining with the endothelial marker CD31 (*green*) revealed a linear pattern of fluorescence surrounded by rAb-53-Cy3 fluorescence (Fig. 6*B*), supporting the localization of rAb-53-Cy3 on astrocyte end feet at the blood-brain barrier adjacent to endothelial cells.

Studies were also done in which brain was injected with rAb-53-Cy3 together with a fluid phase endocytosis marker, Texas Red hydrazide, which is internalized selectively by astrocytes (21). Fig. 6*C* shows a cytoplasmic pattern of Texas Red fluorescence in astrocytes at 3 h, with staining of astrocyte processes extending to the perivascular space. In contrast, rAb-53 labeled with a secondary anti-human antibody (*green*) was seen only in a perivascular pattern. NMO-IgG is thus not internalized by AQP4-expressing astrocytes *in vivo*, but remains largely in astrocyte foot processes at the blood-brain barrier.

Little Internalization of AQP4 in Mouse Brain following Injection of NMO Patient NMO-IgG—To validate the findings obtained with the recombinant monoclonal rAb-53, we studied effects of purified IgG from human NMO and control sera. Treatment of astrocyte cultures for 24 h with NMO-IgG did not affect surface AQP4 expression (Fig. 7*A*) or EAAT2 localization (Fig. 7*B*). IgG from NMO patient sera was also injected into mouse brain; however, its localization cannot be determined because NMO-IgG represents only a small fraction of total IgG. Staining the brain sections with a secondary green anti-human antibody allowed localization of the area of IgG diffusion (Fig. 7*C*). AQP4 localization in this area (*white square*) was determined at different times after injection. AQP4 remained distributed in a perivascular pattern at 20 min and 24 h after injection, both for control and NMO-IgG (Fig. 7*D*). Thus, as found with recombinant antibody, serum NMO-IgG does not cause AQP4 internalization in astrocyte cultures or mouse brain *in vivo*.

DISCUSSION

Although NMO-IgG binding to AQP4 in transfected cell cultures caused internalization of itself and AQP4 by an endocytic mechanism, little or no internalization was found in astrocyte cultures or in brain. We found that NMO-IgG is internalized in several transfected cell lines expressing M1- or M23-AQP4. These results agree with previous work showing internalization of AQP4 in HEK 293 cells transfected with a GFP-AQP4 chi-

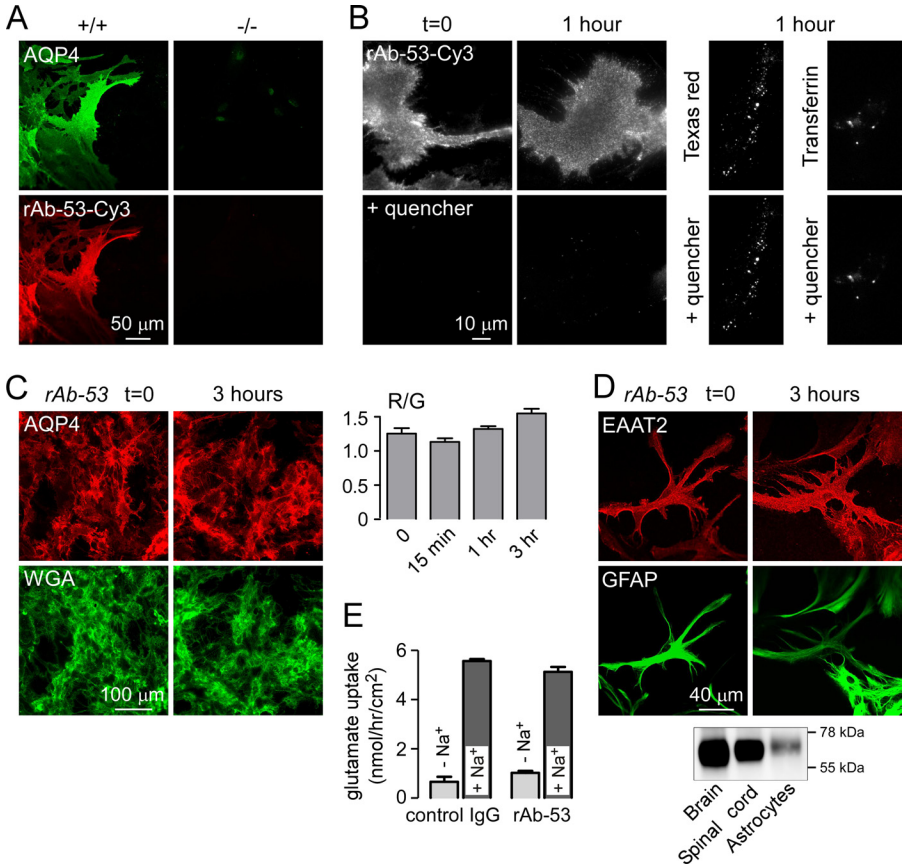

FIGURE 4. **AQP4, rAb-53, and EAAT2 cellular processing in primary astrocyte cultures.** *A*, rAb-53-Cy3 (*red*) binding to AQP4 (*green*) on mouse primary astrocyte cultures. Data are shown for astrocytes from wild type (+/+) and AQP4 null (−/−) mice. *B*, Cy3 fluorescence (*left* and *middle*) before and after addition of quencher, showing minimal internalization of rAb-53-Cy3 at 1-h chase. *Right*, as positive controls for endocytosis, cells incubated for 1 h with Texas Red hydrazide or fluorescein-transferrin. *C*, *left*, cells stained for surface AQP4 (*red*) and plasma membrane (WGA, *green*) at indicated times after incubation with rAb-53 (done as in Fig. 2). *Right*, quantification of surface AQP4 (mean ± S.E. (*error bars*), $n = 10$). *D*, *top*, confocal microscopy showing EAAT2 (*red*) and GFAP (*green*) staining of astrocytes before and after incubation with rAb-53. *Bottom*, EAAT2 immunoblot of mouse brain and spinal cord, and astrocyte cultures. *E*, glutamate uptake in astrocytes preincubated for 24 h with rAb-53 or control IgG (mean ± S.E., $n = 3$). Results are representative of two separate sets of experiments.

mera (12). Interestingly, endocytosis of NMO-IgG and AQP4 in cell cultures was rapid and selective, as internalization was not seen of a Myc antibody upon binding to Myc-tagged AQP4. NMO-IgG internalization, like that of many ligands when bound to their receptors (25), probably involves transduction of the extracellular binding signal to the cytoplasmic endocytosis machinery.

The minimal internalization of NMO-IgG and AQP4 in primary astrocyte cultures found here differs from conclusions of two previous studies (13, 14), where micrographs were reported of a few, fixed/permeabilized cells that were stained for AQP4 after exposure to NMO serum. It is difficult with the prior methods to localize AQP4 confidently, especially in cultured astrocytes that are quite flat, heterogeneous, and have complex morphology. Here, using sensitive, quantitative assays of NMO-IgG-Cy3 internalization and AQP4 surface expression, done on many cells in multiple cell cultures, we found little or no NMO-IgG or AQP4 internalization. The lack of internalization in primary astrocytes was not a consequence of a generally low level of endocytosis because rapid internalization was found for Texas Red hydrazide, a marker of fluid phase endocytosis, and fluorescein-transferrin, a marker of receptor-mediated endocytosis. These findings in astrocyte cell culture are supported by the minimal internalization of NMO-IgG and AQP4 in mouse brain *in vivo*. The localization of rAb-53-Cy3 and AQP4 after intracerebral injection of antibody was strictly perivascular and quite different from that of astrocyte cell bodies as stained by GFAP or internalized Texas Red hydrazide.

The minimal internalization of NMO-IgG and AQP4 on astrocytes *in vivo* and the tight binding of NMO-IgG to AQP4 (22) result in prolonged exposure of NMO-IgG at the cell surface. Exposure of NMO-IgG at the astrocyte surface is predicted to exacerbate NMO pathology, as it would promote the binding and activation of complement and cytotoxic leukocytes. The inefficient endocytosis of NMO-IgG and AQP4 in astrocyte cultures and *in vivo* may be related to astrocyte-specific factors, perhaps the putative macromolecular cell membrane complex containing AQP4, α-syntrophin, dystrophin, and dystroglycans (26), as well as to AQP4 polarization to astrocyte end feet (26, 27), which do not occur in transfected cell culture models.

Loss of AQP4 immunoreactivity is a prominent feature of NMO lesions that is not seen in multiple sclerosis or other neuroinflammatory diseases (28). The proposed mechanisms of AQP4 loss include its endocytosis and targeting for lysosomal degradation and astrocyte loss following complement

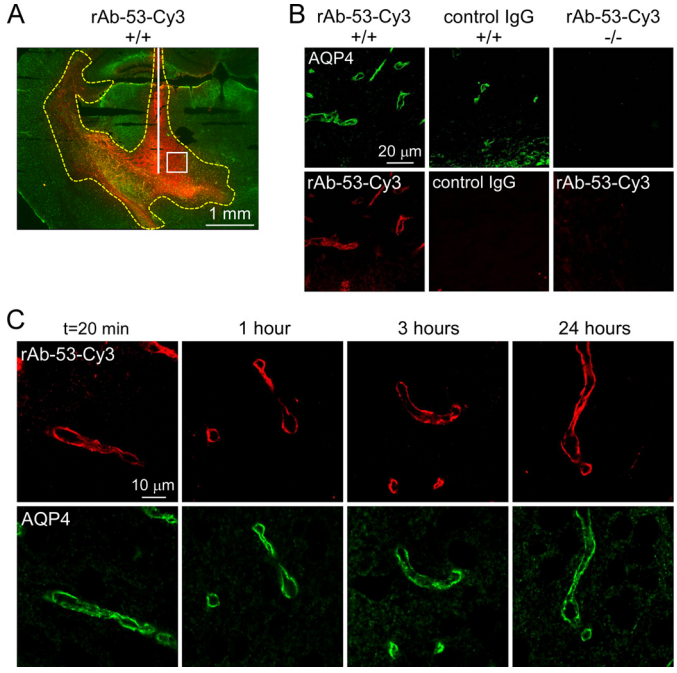

FIGURE 5. **rAb-53 binding to AQP4 *in vivo* following intracerebral injection in mouse brain.** *A*, spatial distribution of rAb-53-Cy3 (*red*) in brain at 3 h after injection. AQP4 stained *green*. *White line*, needle track; *yellow dashed line*, area of rAb-53-Cy3 diffusion; *white square*, area where micrographs in *B* and *C* were obtained. *B*, confocal fluorescence microscopy showing perivascular colocalization of rAb-53-Cy3 (*red*) with AQP4 (*green*) at 3 h after injection in wild-type mice (+/+). Controls included injection of (non-NMO) IgG in wild-type mice and rAb-53-Cy3 in AQP4-null mice (−/−). *C*, localization of rAb-53-Cy3 (*red*) at 20 min and 1, 3, and 24 h after injection, showing perivascular localization with AQP4 (*green*). Micrographs are representative of studies done on 3–4 mice at each time point.

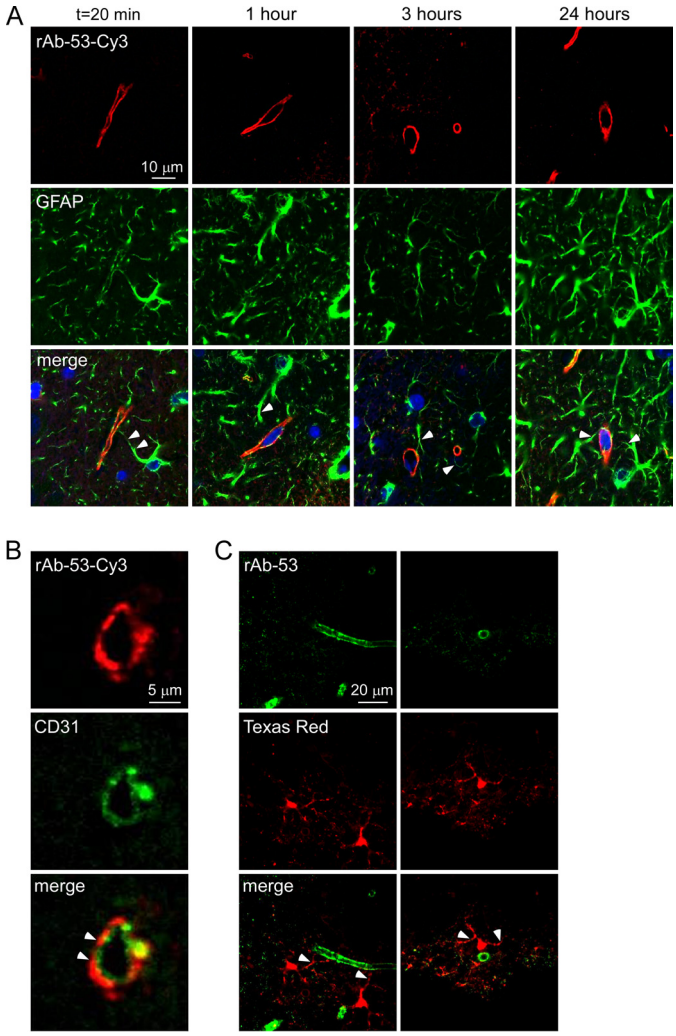

FIGURE 6. **Perivascular astrocyte surface localization of rAb-53 *in vivo* following intracerebral injection.** *A*, confocal microscopy showing rAb-53-Cy3 (*red*) in brain stained for GFAP (*green*) and nuclei (*blue*) at 20 min and 1, 3, and 24 h after injection. *Arrowheads* in *merge image* indicate astrocytes stained for GFAP whose processes extend to the perivascular space. *B*, confocal microscopy showing rAb-53-Cy3 (*red*) and the endothelial marker CD31 (*green*) at 3 h after injection. *Arrowheads* indicate rAb-53-Cy3 surrounding CD31. *C*, confocal microscopy at 3 h after injection of Texas Red hydrazide (a dye internalized by astrocytes, *red*) and rAb-53 (stained with a secondary anti-human antibody, *green*). *Arrowheads* indicate astrocyte foot processes extending to the perivascular space.

and cell-mediated cytotoxicity. The parallel loss of GFAP and AQP4 supports the second mechanism, as does our finding of minimal AQP4 internalization *in vivo* even following exposure to large amounts of NMO-IgG in the form of a pathogenic recombinant monoclonal antibody or of IgG from human NMO sera. Moreover, if coinjected into brain with human complement, the NMO-IgG as used here produces NMO-like lesions with loss of AQP4, GFAP, and myelin, leukocyte infiltration, and deposition of activated complement (7). However, intracerebral injection of NMO-IgG without complement does not cause loss of AQP4 immunoreactivity (7). A therapy-relevant consequence of our findings is that NMO pathology is predicted to be reduced by maneuvers that lower expression of AQP4 on the astrocyte surface or promote its internalization following NMO-IgG binding, perhaps by interfering with polarization mechanisms.

We found no significant internalization of glutamate transporter EAAT2 on astrocytes after exposure to high concentrations of NMO-IgG, both by EAAT2 immunofluorescence and by functional assay of glutamate uptake. EAAT2 and AQP4 cointernalization were previously demonstrated in AQP4-transfected HEK-293 cells (13). Perhaps AQP4 overexpression in HEK-293 cells produced interactions between EAAT2 and AQP4 that do not occur in astrocytes. In the same study (13), the reported reduction in EAAT2 and AQP4 expression in spinal cord of NMO patients may be related to astrocyte loss rather than cointernalization of AQP4 and EAAT2. Although we think it unlikely, our data do not rule out the involvement of glutamate excitotoxicity in NMO because impaired glutamate uptake might occur by astrocyte loss rather than EAAT2 internalization. Mice deficient in EAAT2 show lethal spontaneous seizures and increased susceptibility to acute cortical injury due to elevated levels of glutamate in brain (20). EAAT2 internalization, if it occurred, would be predicted to produce a seizure phenotype, which is not found clinically in NMO. We conclude that EAAT2 up-regulation by ceftriaxone would not have therapeutic utility in NMO.

In conclusion, our data challenge two widely cited mechanisms of NMO disease pathogenesis: NMO-IgG-induced AQP4 internalization and NMO-IgG-induced EAAT2 internalization. The continued exposure of NMO-IgG-bound AQP4 at the astrocyte cell surface in NMO is likely an important mechanism in NMO pathogenesis because it provides a

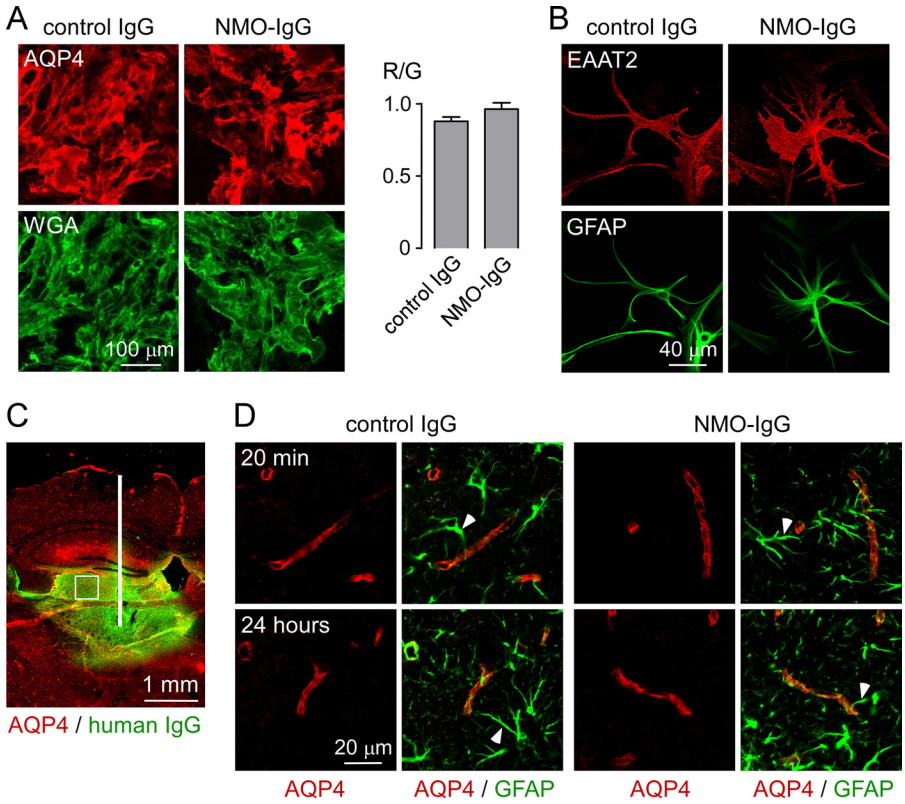

FIGURE 7. **Perivascular astrocyte membrane localization of AQP4 *in vivo* following intracerebral injection of purified IgG from NMO sera.** A, *left*, mouse astrocytes stained for surface AQP4 (*red*) and plasma membrane (WGA, *green*) after a 24-h incubation with purified IgG from NMO or control sera (done as in Fig. 2). *Right*, quantification of surface AQP4 (mean ± S.E. (*error bars*), $n = 10$). *B*, EAAT2 (*red*) and GFAP (*green*) staining of astrocytes after 24-h incubation with control or NMO-IgG. *C*, intracerebral injection. Brain section stained for human IgG (*green*, showing area of diffusion) and AQP4 (*red*). *White line*, needle tract; *white square*, area where AQP4 localization was assessed in *D*. *D*, confocal micrographs of AQP4 (*red*) and GFAP (*green*) at 20 min and 24 h after injection of control or NMO-IgG. *Arrowheads* indicate GFAP-stained astrocyte foot processes. Results are representative of micrographs from 2–4 mice per condition.

continued focus for cytotoxic complement and leukocyte interactions.

REFERENCES

1. Jarius, S., and Wildemann, B. (2010) *Nat. Rev. Neurol.* **6,** 383–392
2. Wingerchuk, D. M., Lennon, V. A., Lucchinetti, C. F., Pittock, S. J., and Weinshenker, B. G. (2007) *Lancet Neurol.* **6,** 805–815
3. Lennon, V. A., Kryzer, T. J., Pittock, S. J., Verkman, A. S., and Hinson, S. R. (2005) *J. Exp. Med.* **202,** 473–477
4. Lennon, V. A., Wingerchuk, D. M., Kryzer, T. J., Pittock, S. J., Lucchinetti, C. F., Fujihara, K., Nakashima, I., and Weinshenker, B. G. (2004) *Lancet* **364,** 2106–2112
5. Hinson, S. R., McKeon, A., and Lennon, V. A. (2010) *Neuroscience* **168,** 1009–1018
6. Verkman, A. S., Ratelade, J., Rossi, A., Zhang, H., and Tradtrantip, L. (2011) *Acta Pharmacol. Sin.* **32,** 702–710
7. Saadoun, S., Waters, P., Bell, B. A., Vincent, A., Verkman, A. S., and Papadopoulos, M. C. (2010) *Brain* **133,** 349–361
8. Bennett, J. L., Lam, C., Kalluri, S. R., Saikali, P., Bautista, K., Dupree, C., Glogowska, M., Case, D., Antel, J. P., Owens, G. P., Gilden, D., Nessler, S., Stadelmann, C., and Hemmer, B. (2009) *Ann. Neurol.* **66,** 617–629
9. Bradl, M., Misu, T., Takahashi, T., Watanabe, M., Mader, S., Reindl, M., Adzemovic, M., Bauer, J., Berger, T., Fujihara, K., Itoyama, Y., and Lassmann, H. (2009) *Ann. Neurol.* **66,** 630–643
10. Kinoshita, M., Nakatsuji, Y., Kimura, T., Moriya, M., Takata, K., Okuno, T., Kumanogoh, A., Kajiyama, K., Yoshikawa, H., and Sakoda, S. (2009) *Biochem. Biophys. Res. Commun.* **386,** 623–627
11. Zhang, H., Bennett, J. L., and Verkman, A. S. (August 2, 2011) *Ann. Neurol.* 10.1002/ana.22551
12. Hinson, S. R., Pittock, S. J., Lucchinetti, C. F., Roemer, S. F., Fryer, J. P., Kryzer, T. J., and Lennon, V. A. (2007) *Neurology* **69,** 2221–2231
13. Hinson, S. R., Roemer, S. F., Lucchinetti, C. F., Fryer, J. P., Kryzer, T. J., Chamberlain, J. L., Howe, C. L., Pittock, S. J., and Lennon, V. A. (2008) *J. Exp. Med.* **205,** 2473–2481
14. Vincent, T., Saikali, P., Cayrol, R., Roth, A. D., Bar-Or, A., Prat, A., and Antel, J. P. (2008) *J. Immunol.* **181,** 5730–5737
15. Marignier, R., Nicolle, A., Watrin, C., Touret, M., Cavagna, S., Varrin-Doyer, M., Cavillon, G., Rogemond, V., Confavreux, C., Honnorat, J., and Giraudon, P. (2010) *Brain* **133,** 2578–2591
16. Rothstein, J. D., Patel, S., Regan, M. R., Haenggeli, C., Huang, Y. H., Bergles, D. E., Jin, L., Dykes Hoberg, M., Vidensky, S., Chung, D. S., Toan, S. V., Bruijn, L. I., Su, Z. Z., Gupta, P., and Fisher, P. B. (2005) *Nature* **433,** 73–77
17. Ma, T., Yang, B., Gillespie, A., Carlson, E. J., Epstein, C. J., and Verkman, A. S. (1997) *J. Clin. Invest.* **100,** 957–962
18. Crane, J. M., Van Hoek, A. N., Skach, W. R., and Verkman, A. S. (2008) *Mol. Biol. Cell* **19,** 3369–3378
19. Li, L., Zhang, H., Varrin-Doyer, M., Zamvil, S. S., and Verkman, A. S. (2011) *FASEB J.* **25,** 1556–1566
20. Tanaka, K., Watase, K., Manabe, T., Yamada, K., Watanabe, M., Takahashi, K., Iwama, H., Nishikawa, T., Ichihara, N., Kikuchi, T., Okuyama, S., Kawashima, N., Hori, S., Takimoto, M., and Wada, K. (1997) *Science* **276,** 1699–1702
21. Nimmerjahn, A., Kirchhoff, F., Kerr, J. N., and Helmchen, F. (2004) *Nat. Methods* **1,** 31–37
22. Crane, J. M., Lam, C., Rossi, A., Gupta, T., Bennett, J. L., and Verkman, A. S. (2011) *J. Biol. Chem.* **286,** 16516–16524
23. Crane, J. M., Tajima, M., and Verkman, A. S. (2010) *Neuroscience* **168,** 892–902
24. Skytt, D. M., Madsen, K. K., Pajcka, K., Schousboe, A., and Waagepetersen, H. S. (2010) *Neurochem. Res.* **35,** 2043–2052

25. Sorkin, A., and von Zastrow, M. (2009) *Nat. Rev. Mol. Cell. Biol.* **10,** 609–622
26. Neely, J. D., Amiry-Moghaddam, M., Ottersen, O. P., Froehner, S. C., Agre, P., and Adams, M. E. (2001) *Proc. Natl. Acad. Sci. U.S.A.* **98,** 14108–14113
27. Frigeri, A., Gropper, M. A., Umenishi, F., Kawashima, M., Brown, D., and Verkman, A. S. (1995) *J. Cell Sci.* **108**, 2993–3002
28. Misu, T., Fujihara, K., Kakita, A., Konno, H., Nakamura, M., Watanabe, S., Takahashi, T., Nakashima, I., Takahashi, H., and Itoyama, Y. (2007) *Brain* **130,** 1224–1234
29. Valentine, C. D., Verkman, A. S., and Haggie, P. M. (2011) *Traffic* doi: 10.1111/j.1600-0854.2011.01287.x